IEEE Robotics and Automation Letters (RAL) paper presented at the
2020 IEEE/RSJ International Conference on Intelligent Robots and Systems (IROS)
October 25-29, 2020, Las Vegas, NV, USA (Virtual)

Modeling and Experimental Verification of a Cable-Constrained Synchronous Rotating Mechanism Considering Friction Effect

Yanan Li, Yu Liu, Deshan Meng, Member, IEEE, Xueqian Wang, Bin Liang

***Abstract*— Cable-Constrained Synchronous Rotating Mechanism (CCSRM) has an important application prospect in the field of cable-driven robots, which can greatly reduce the number of driving motors while ensuring the light and slender body. However, there are obvious cable friction effect and elastic deformation in CCSRM. These nonlinear characteristics have a significant impact on synchronous motion performance. In this paper, a model of CCSRM considering cable friction is proposed, which integrates the effects of cable pretension, elastic deformation, and friction between cable and pulley on system characteristics. The distribution law of cable tension under the influence of friction force and the phenomenon of motion hysteresis caused in reverse rotation are emphatically discussed. Then, an improved LuGre friction model is proposed to solve the problem of line contact friction between cables and pulleys. Further a dynamic model of CCSRM is established to simulate the motion characteristics of the whole process, including the discontinuous friction phenomenon in reverse rotation. Finally, an experimental prototype of two-axis synchronous rotating system is built, and the friction coefficient is identified. The experimental results show that the dynamic model can well simulate the motion characteristics of CCSRM.**

I. INTRODUCTION

Cable-driven robots, inspired by the natural organs such as elephant trunk and octopus arm, have a slim light body and super-redundant degree of freedoms (DOFs) [1], [2]. Therefore, they have a wide application prospect in narrow space environments [3], [4], such as nuclear plants maintenance [5], in-space inspection [6], parts assembly [7] and other fields [8]. Some scholars have studied the use of super-elastic structure as ridgelines of cable-driven robots [9], [10]. The structure of this type of robot is relatively simple, and the modeling work focuses on the handling of elastic support rods [11], [12].

This work was supported by the National Natural Science Foundation of China (Grant No. 61903215), the Guangdong Natural Science Foundation(Grant 2018A030310679), the Basic Research Program of Shenzhen (JCYJ20180306174321766).*(Corresponding authors: Yu Liu; Deshan Meng.)*

Yanan Li is with Harbin Institute of Technology, Harbin 150000, China, and also with the Shenzhen International Graduate School, Tsinghua University, Shenzhen 518055, China(e-mail: 19B308004@stu.hit.edu.cn).

Yu Liu is with Harbin Institute of Technology, Harbin 150000, China(e-mail: lyu11@hit.edu.cn).

Deshan Meng is with School of Aeronautics and Astronautics, Sun Yat-Sen University, Guangzhou 510275, China, and also with the Shenzhen International Graduate School, Tsinghua University, Shenzhen 518055, China(e-mail: dsmeng16@foxmail.com).

Xueqian Wang and Bin Liang are with the Shenzhen International Graduate School, Tsinghua University, Shenzhen 518055, China(e-mail: wang.xq@sz.tsinghua.edu.cn; liangbin@tsinghua.edu.cn).

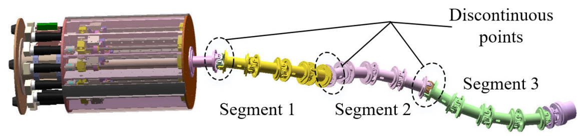

Fig. 1. The segmented manipulator composed of CCSRM.

However, the stiffness and load capacity of this type of robot is relatively low due to its structural elasticity [13]. Liu et al. [14] proposes a cable-driven manipulator shown in Fig. 1, which is composed of rigid links and traditional joints. Its biggest bright spot is to achieve synchronous rotation of adjacent joints through CCSRM. As shown in Fig. 1, the segmented manipulator composed of CCSRM can approximately simulate equal curvature bending of continuum robots. The CCSRM can not only realize the miniaturization of manipulator's size, which is very important for robots working in narrow space, but also can obtain high stiffness and large load capacity of manipulators. However, due to the introduction of many linkage cables, the complexity of the robot system has greatly increased, which has higher requirements for system modeling. Liu et al. only discusses the design and kinematics of CCSRM, while statics and dynamics related to synchronous rotation performance is not explored. On the basis of the work in [14], Ma et al. [15] carries out the work about dynamics modeling and analysis of cable-driven manipulator composed of CCSRM. For the modeling of CCSRM, Ma et al. refer to Closed Cable Loops (CCL) model of solar array's deployment mechanism [16], [17] and regard linkage as linear torsion spring constraint. In the CCL model, only the cable stiffness characteristics are considered [18], [19].

Different from the solar array's deployment mechanism, the CCSRM in the robot needs to move back and forth for many times, and requires higher precision. Therefore, in the robot system, it is necessary to carry out more delicate handling of cables, such as the influence of cable friction on tension distribution. Agrawal et al. [20] conducted a detailed study on the tension transmission characteristics in the cable-conduit system using static Coulomb friction model. Do et al. [21], [22] uses modified LuGre model and normalized Bouc–Wen model to describe friction characteristics between the tendon and sheath, while under the condition that no change of the accumulated curve angle occurs during the operation. These studies show that friction has a significant effect on the performance of systems with cables. Also for

CCSRM, the effect of cable friction on synchronous rotation accuracy cannot be ignored and a dynamic friction model suitable for CCSRM needs to be built.

Due to the design limitation of the slender structure, this type of robot often lacks corresponding feedback at the distal end. Therefore, the model considering friction can be used in the compensation control of the system. Do et al. [23] designed a feedforward controller to compensate for the hysteresis in the surgical robot through the established hysteresis model. Agrawal et al. [24] proposes an adaptive robust control method while utilizing the limited output feedback available in conjunction with the intermediate actuator position feedback.

In this paper, we carry out a detailed study on the statics and dynamics of CCSRM and elaborate two contributions. First, a refined model of CCSRM with friction is proposed. The model can simulate the motion characteristics of synchronous rotating mechanism more truly. Second, an improved LuGre friction model is used to solve the line contact friction problem of cable-pulley, which can accurately reflect the friction change of the cable passing through the pulley. On this basis, the dynamic model of the cable synchronous rotation mechanism is established.

The remainder of this paper is organized as follows. Section II elaborates the research issues in this paper. In section III, the statics model of CCSRM is established, and the joint stiffness and hysteresis characteristics are analyzed. Section IV establishes the dynamics model of CCSRM. In section V, an experimental prototype is developed. Typical experiments are performed to verify the established model. The last section summarizes the whole paper and gives the conclusions.

II. MOTIVATION

As shown in Fig. 1, the manipulator has three segments, each segment contains multiple joints. The adjacent joints in the same segment are connected by cables in a specific way to realize rotation at approximately equal angles, which is similar to the equal curvature bending of the continuum robot. This can improve the flexibility of the segmented manipulator, and achieve a higher stiffness compared with continuum robots. Table I presents a list of nomenclature used throughout this paper.

A. Introduction to Principle of CCSRM

As part of the manipulator, the CCSRM is the basic unit and composed of a pair of agonist and ant-agonist cables and two pairs of pulleys, as shown in Fig. 2. These cables are called Coupling Cable Pairs (CCP), and each pair consists of two 'S' shaped cables that are placed crosswise around the pulleys. The anchors of the cables are fixed on $Link_{i-1}$ and $Link_{i+1}$. The pulleys are fixed on $Link_i$ and are concentric with the joint axis. As the two cables are antisymmetric, take one cable as an example. As shown in Fig. 3, points A_1 and A_2 are cable anchors, each coupling cable is artificially divided into five parts according to whether it is in contact with the pulley. When the joint rotates, the length of L_1, L_2, L_3 (yellow color) will remain constant for they are always along the tangent direction of the pulley. Only the winding parts of the cable, denoted $\widehat{S}_1$ and $\widehat{S}_2$ (red color), will change. When the rotation angle of joint i is θ_i, the rotation angle of joint $i+1$ is θ_{i+1}, the winding parts of the cable become $\widehat{S}_1'$ and $\widehat{S}_2'$, respectively.

$$\begin{aligned} \widehat{S}_1' &= \widehat{S}_1 - r\theta_i \\ \widehat{S}_2' &= \widehat{S}_2 + r\theta_{i+1} \end{aligned} \tag{1}$$

where r is the radius of the pulley.

TABLE I

NOMENCLATURE TABLE

	Geometric Relationship
$L_{(\cdot)}$	Length of non-contact part of cable and pulley
$\widehat{S}_{(\cdot)}$	Length of contact part of cable and pulley
r	Pulley radius
	Statics Modeling
$\theta_{(\cdot)}$,$\dot{\theta}_{(\cdot)}$	Joint angle and angular velocity
$\Delta\theta$,$\Delta\theta^{(\cdot)}$	Synchronous rotation error in different states
Δl	Cable deformation
k	Cable elastic coefficient
T,$T_{(\cdot)}$	Cable tension
T_p	Cable pretention
θ_{w0}	Cable initial wrap angle
$\theta_{\mathrm{wrap}(\cdot)}$	Cable pulley wrap angle
$\eta_{(\cdot)}$	Cable tension transfer coefficient
k_{equal},$k_{\mathrm{equal}}^{(\cdot)}$	Joint equivalent stiffness in different states
	Dynamics Modeling
sign($\cdot$),sat($\cdot$)	Sign and saturation function
f_c,f_s,v_s,σ_0,σ_1,σ_2	LuGre friction model parameters
$g(v)$	Stribeck function
ε	A small damping item
J	Link inertia

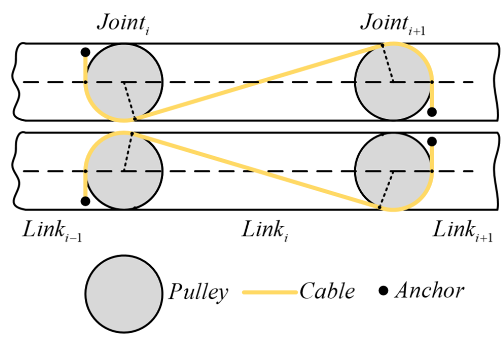

Fig. 2. Cable pulley synchronous rotation unit.

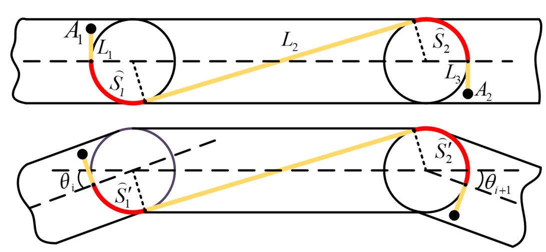

Fig. 3. Length change of cable winding part.

Assuming that the total length of the cable remains the same, the following relation can be obtained:

$$\widehat{S}_1' + \widehat{S}_2' = \widehat{S}_1 + \widehat{S}_2 \tag{2}$$

Combining Eq. (1) and Eq. (2) yields:

$$r\left(\theta_i - \theta_{i+1}\right) = 0 \tag{3}$$

That is, the angles of joint i and joint $i+1$ are always equal in theory.

B. Motivation

According to the linkage design principle of the CCSRM, one of the preconditions for realizing complete synchronization of adjacent joints is that the length of cables is unchanged, that is, the cables cannot deform. However, the cable will inevitably deform under complex stress conditions, resulting in the change of cable length. Therefore, the main factors that affect the synchronous rotation accuracy of the CCSRM include the cable stiffness, cable tension distribution.

The friction force between the cable and pulley has an impact on the cable tension distribution. Therefore, if the motion characteristics of the CCSRM are to be accurately described, the influence of friction must be fully considered. Synchronous rotation accuracy will directly affect the positioning accuracy of robots, so it is very important to establish fine models of the CCSRM, including statics and dynamics. On one hand, they can be used to deeply analyze the motion characteristics of the CCSRM and guide the improvement of the design. On the other hand, they can assist the control of the robot and improve its motion performance.

III. STATICS MODELING

A. Statics Modeling without Friction

When the CCSRM moves, one cable gradually tightens while the other loosens. Therefore, in order to prevent the cable from sagging, the cable must apply a certain initial pretension force T_p. Since winding sections ($\widehat{S}_1$ and $\widehat{S}_2$) and fixed sections (L_1 and L_3) are relatively short, only consider the deformation of the section L_2. The cable tension is calculated as follows:

$$\begin{aligned} T_1 &= T_p - k\Delta l \\ T_2 &= T_p + k\Delta l \end{aligned} \tag{4}$$

where T_1 and T_2 are cable tension of CCP. Δl is the cable deformation. When Δl is positive, cable 1 is loosening and cable 2 is tightening. k is elastic coefficient of the cable, and $k = EA/l_0$, E, A, l_0 are the elastic modulus, cross-sectional area and length of the cable.

The deformation of cable is calculated as follows:

$$\begin{aligned} \Delta l &= \widehat{S}_1 + \widehat{S}_2 - \left(\widehat{S}_1' + \widehat{S}_2'\right) = r\Delta\theta \\ \Delta\theta &= \theta_2 - \theta_1 \end{aligned} \tag{5}$$

where $\Delta\theta$ is the synchronous rotation error of adjacent joints. θ_1 and θ_2 are angles of joint 1 and joint 2, respectively. By using the virtual work principle, the energy conservation equation can be obtained as follows:

$$\tau\delta\theta = \left(T_2 - T_1\right)\delta(\Delta l) \tag{6}$$

The rotation angle and cable deformation have the following relationship:

$$\tfrac{\delta(\Delta l)}{\delta\theta} = r \tag{7}$$

Combining Eq. (6) with Eq. (7), the tension-torque relationship of the CCP is obtained:

$$\tau_c = \left(T_2 - T_1\right) r = 2kr^2\Delta\theta \tag{8}$$

Define the equivalent stiffness of synchronous joint:

$$k_{\text{equal}} = 2kr^2 \tag{9}$$

The equivalent stiffness of joint is only related to the elastic coefficient of cable and the radius of pulley. However, friction is ignored in the modeling process. Therefore, Eq. (8) cannot fully describe characteristics of the system.

B. Friction Model between Cable and Pulley

There is a line contact between the cable and the pulley, instead of point contact. The cable tension is changed on both sides of the pulley due to friction force. The static friction model of the cable-pulley is often deduced based on the Coulomb friction model.

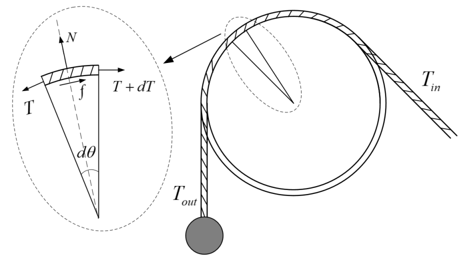

Fig. 4. Infinitesimal cable-pulley element.

As shown in Fig. 4, analysis infinitesimal cable-pulley element:

$$\begin{aligned} N &= Td\theta \\ dT &= -f = -u_c T d\theta \,\mathrm{sign}(v) \end{aligned} \tag{10}$$

where T is the cable tension, $d\theta$ and dT are the wrap angle and the cable tension difference on both sides corresponding to the micro element. N is normal force, f is the friction of the cable on the pulley. v is the relative speed and u_c is Coulomb friction coefficient, $\mathrm{sign}(v)$ is sign function defined as follows:

$$\mathrm{sign}(v) = \begin{cases} 1 & v > 0 \\ -1 & v < 0 \end{cases} \tag{11}$$

The first order differential equation of the cable tension is obtained by Eq. (10):

$$\tfrac{dT}{T} = -u_c\,\mathrm{sign}(v)d\theta \tag{12}$$

By integrating the Eq. (12) to get the cable-pulley tension transmission:

$$T_{\text{out}} = T_{\text{in}}\eta = T_{\text{in}} e^{-u_c\theta_{\text{wrap}}\,\mathrm{sign}(v)} \tag{13}$$

where T_{in} and T_{out} are tension input and output on both sides of pulley, θ_{wrap} is wrap angle. η represents the cable tension transfer coefficient, with $\eta = e^{-u_c\theta_{\text{wrap}}\,\text{sign}(v)}$.

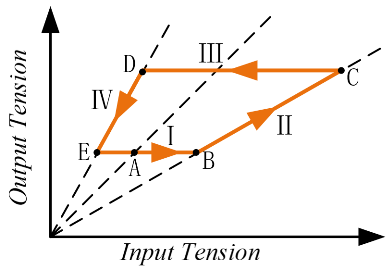

Fig. 5. Cable-pulley tension transmission.

Assuming that the wrap angle is constant, the meaning of the Eq. (13) can be shown in Fig. 5. The cable tension transmission is divided into four stages. Stage II and stage IV represent the tension loading and unloading stages, respectively. Stage I and stage III represent friction direction changing stages. Assuming that the cable tensions on both sides of the pulley are equal at the initial moment, which means the cable is only attached to the pulley, and the friction of the cable-pulley is zero, corresponding to point A. When the input tension increases gradually, the output tension remains unchanged due to the frictional force until it reaches point B. Then the tension transfer relationship satisfies the Eq. (13) with $v > 0$. Then the input tension is gradually reduced at point C, the direction of friction is gradually changed, whille the output tension remains unchanged until moment D, and satisfies the Eq. (13) with $v < 0$ and starts to move.

C. Statics Modeling with Friction

In order to describe the static transmission relationship of CCSRM more accurately, we further established the statics model of CCSRM considering friction. As shown in the Fig. 6, each cable is in contact with the pulley twice. The tension of cable 1 in sections L_1, L_2, L_3 are defined as T_{11}, T_{12}, T_{13}, respectively. Similarly, the tensions of cable 2 are defined as T_{21}, T_{22}, T_{23}.

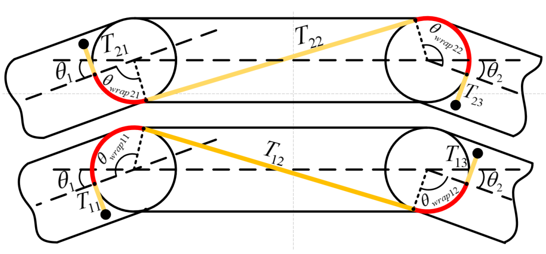

Fig. 6. Tension distribution and wrap angle.

Combining the cable-pulley tension transmission Eq. (13), the cable tension distribution is obtained as:

$$\begin{array}{cc} T_{11} = T_{12}/\eta_{11} & T_{21} = T_{22}\eta_{21} \\ T_{12} = T_p - k\Delta l & T_{22} = T_p + k\Delta l \\ T_{13} = T_{12}\eta_{12} & T_{23} = T_{22}/\eta_{22} \end{array} \tag{14}$$

where tension transmission coefficients satisfy the following relations:

$$\begin{aligned} \eta_{11} &= e^{-u\theta_{\text{wrap11}}\,\text{sign}(\dot\theta_1)}, \eta_{12} = e^{-u\theta_{\text{wrap12}}\,\text{sign}(\dot\theta_2)} \\ \eta_{21} &= e^{-u\theta_{\text{wrap21}}\,\text{sign}(\dot\theta_1)}, \eta_{22} = e^{-u\theta_{\text{wrap22}}\,\text{sign}(\dot\theta_2)} \end{aligned} \tag{15}$$

As shown in Fig. 6, wrap angles are calculated as follows:

$$\begin{aligned} \theta_{\text{wrap11}} &= \theta_{\text{w0}} + \theta_1, \theta_{\text{wrap12}} = \theta_{\text{w0}} - \theta_2 \\ \theta_{\text{wrap21}} &= \theta_{\text{w0}} - \theta_1, \theta_{\text{wrap22}} = \theta_{\text{w0}} + \theta_2 \end{aligned} \tag{16}$$

where θ_{w0} is the initial wrap angle. The tension difference between two cables is:

$$\begin{aligned} \Delta T &= T_{21} - T_{11} \\ &= [T_p + k\Delta l]\,\eta_{21} - [T_p - k\Delta l]/\eta_{11} \end{aligned} \tag{17}$$

Combining Eq. (15), Eq. (16) and Eq. (17):

$$\begin{aligned} \Delta T =& e^{u\theta_1\,\text{sign}(\dot\theta_1)}\left(e^{u\theta_{\text{w0}}\,\text{sign}(\dot\theta_1)} + e^{-u\theta_{\text{w0}}\,\text{sign}(\dot\theta_1)}\right)k\Delta l \\ &+ e^{u\theta_1\,\text{sign}(\dot\theta_1)}T_p\left(e^{-u\theta_{\text{w0}}\,\text{sign}(\dot\theta_1)} - e^{u\theta_{\text{w0}}\,\text{sign}(\dot\theta_1)}\right) \end{aligned} \tag{18}$$

Link 1 is driven passively by CCP, so the cable tension difference can be regarded as the joint driving force. Similar to the Eq. (8), the relationship of cable tension-torque is obtained:

$$\begin{aligned} \tau_c &= \Delta T r \\ =& e^{u\theta_1\,\text{sign}(\dot\theta_1)}\left(e^{u\theta_{\text{w0}}\,\text{sign}(\dot\theta_1)} + e^{-u\theta_{\text{w0}}\,\text{sign}(\dot\theta_1)}\right)kr^2\Delta\theta \\ &+ e^{u\theta_1\,\text{sign}(\dot\theta_1)}T_p\left(e^{-u\theta_{\text{w0}}\,\text{sign}(\dot\theta_1)} - e^{u\theta_{\text{w0}}\,\text{sign}(\dot\theta_1)}\right)r \end{aligned} \tag{19}$$

When $\dot\theta_1 > 0$ and $\tau_c = 0$, it is called static equilibrium state I, then:

$$\left(e^{u\theta_{\text{w0}}} + e^{-u\theta_{\text{w0}}}\right)kr\Delta\theta^+ + T_p\left(e^{-u\theta_{\text{w0}}} - e^{u\theta_{\text{w0}}}\right) = 0 \tag{20}$$

where $\Delta\theta^+$ is the joint synchronous rotation error of the static equilibrium state I. Then the joint 1 is fixed and an infinitely small external force is exerted on the joint 1:

$$\begin{aligned} \delta\tau =& e^{u\theta_1}\left(e^{u\theta_{\text{w0}}} + e^{-u\theta_{\text{w0}}}\right)kr^2\left(\Delta\theta^+ + \delta\theta\right) \\ &+ e^{u\theta}T_p\left(e^{-u\theta_{\text{w0}}} - e^{u\theta_{\text{w0}}}\right)r \\ =& e^{u\theta_1}\left(e^{u\theta_{\text{w0}}} + e^{-u\theta_{\text{w0}}}\right)kr^2\delta\theta \end{aligned} \tag{21}$$

The equivalent stiffness of the joint is:

$$k^+_{\text{equal}} = \frac{\delta\tau}{\delta\theta} = e^{u\theta_1}\left(e^{u\theta_{\text{w0}}} + e^{-u\theta_{\text{w0}}}\right)kr^2 \tag{22}$$

When the joint rotates in the opposite direction, $\dot\theta_1 < 0$ and $\tau_c = 0$, it is called static equilibrium state II, then:

$$\left(e^{u\theta_{\text{w0}}} + e^{-u\theta_{\text{w0}}}\right)kr\Delta\theta^- + T_p\left(e^{u\theta_{\text{w0}}} - e^{-u\theta_{\text{w0}}}\right) = 0 \tag{23}$$

where $\Delta\theta^-$ is the joint synchronous rotation error of the static equilibrium state II. The equivalent joint stiffness of the joint inverse movement can also be obtained:

$$k^-_{\text{equal}} = e^{-u\theta_1}\left(e^{u\theta_{\text{w0}}} + e^{-u\theta_{\text{w0}}}\right)kr^2 \tag{24}$$

It can be seen that the equivalent stiffness of the joint is not only related to the elastic coefficient of cable and the radius of pulley, but also the friction coefficient and the initial wrap angle. In addition, the stiffness of the manipulator is also related to the rotation angle of joint. Therefore, the equivalent stiffness varies with the configuration of robot. When the movement direction of the joint changes, the joint stiffness changes dramatically. The Fig. 7 shows the joint stiffness with the relationship of joint angle and angular velocity.

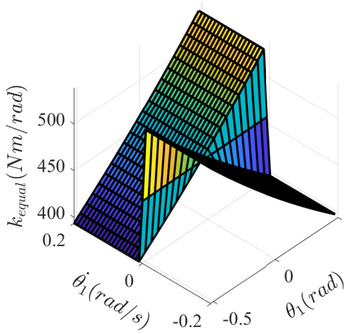

Fig. 7. Joint stiffness with joint angle and angular velocity.

Since the joint 2 is driving joint and joint 1 is passive joint. When joint 2 starts to rotate in the opposite direction, joint 1 will not immediately rotate in the opposite direction until the direction of the friction force changes. Similar to the backlash with gear transmission, the difference in rotation angle of joint 2 can be regarded as the backlash of the cable pulley transmission system.

$$\Delta\theta^{+} - \Delta\theta^{-} = \frac{2T_p\left(e^{u\theta_{w0}} - e^{-u\theta_{w0}}\right)}{\left(e^{u\theta_{w0}} + e^{-u\theta_{w0}}\right)kr} \tag{25}$$

The cable-pulley friction makes the robot have a large transmission hysteresis when the movement direction changes. The transmission backlash is related to the initial pretension of the cable and the initial wrap angle. Increasing the radius of the pulley or the stiffness of the cable can reduce the transmission backlash.

IV. DYNAMICS MODELING

A. An Improved LuGre Dynamic Friction Model

The friction model of the cable pulley obtained by Eq. (13) does not consider the situation that the relative velocity is equal to zero. The friction is discontinuous when the velocity direction changes. It is unable to deal with the friction change in the process of joint reverse movement. Rone et al. [25] uses the saturation function to replace the sign function, so that the friction force is continuous at the speed equal to zero.

$$\operatorname{sat}(v) = \begin{cases} v/v_{\text{threshold}} & |v| < v_{\text{threshold}} \\ \operatorname{sign}(v) & |v| \geq v_{\text{threshold}} \end{cases} \tag{26}$$

Palli et al. [26] uses $\tanh(v)$ to avoid numerical problems in simulation. However, these models are all static friction models and cannot simulate Stribeck effect and hysteresis that occur in the system. The LuGre [27] model is a dynamic friction model, which can give a more realistic description of friction changes.

$$\begin{aligned} f &= \sigma_0 z + \sigma_1 \dot{z} + \sigma_2 v \\ \dot{z} &= v - \frac{\sigma_0 |v|}{g(v)} z \\ g(v) &= f_c + (f_s - f_c)\, e^{-(v/v_i)^2} \end{aligned} \tag{27}$$

where f is the friction force and z is the state variable that denotes the average bristle deflection. v is the relative velocity of the two contact surfaces. The function models the Stribeck effect and $g(v) > 0$. σ_0, σ_1 and σ_2 are elastic stiffness, damping and viscous friction parameter, respectively. f_c and f_s are Coulomb friction and the maximum static friction, respectively. v_s is Stribeck velocity.

The cable and pulley are in line contact, and the calculation of the friction needs to be integrated along the pulley path. In order to extend the LuGre model to a line contact dynamic friction model, several improvements have been made to the LuGre model given in Eq. (27). The basic idea is to take the friction force as a whole, equivalent LuGre model parameters are obtained by combining cable-pulley static friction model, thus the LuGre friction model is extended to dynamic friction model suitable for calculating cable-pulley friction.

Improvement 1: Combining the Eq. (13), the equivalent Coulomb friction force is obtained ,with $f_c = T_{\text{in}} - T_{\text{out}} = T_{\text{in}}\left(1 - e^{-u_c\theta_{\text{wrap}}\operatorname{sign}(v)}\right)$. In addition, a sufficiently small damping term ε is added to avoid the numerical problems.

$$f_c = T_{\text{in}} - T_{\text{out}} = T_{\text{in}}\left(1 - e^{-u_c\theta_{\text{wrap}}\operatorname{sign}(v)}\right) + \varepsilon \tag{28}$$

Improvement 2: Since the static friction force is difficult to obtain, the friction coefficient is determined by the material of the two contact surfaces, the equivalent maximum static friction force is defined as follows:

$$f_s = \tfrac{u_s}{u_c} f_c \tag{29}$$

where u_s is coefficient of static friction.

B. Dynamics and Numerical Simulation

Generally, the input of dynamics is the motor drive torque. For the synchronous rotation test platform, joint 2 is the active drive joint and joint 1 is the passive drive joint. For joint 1, the torque generated by the cable force is the joint drive torque, and the cable tension-torque relationship is

$$\tau_c = (T_{21} - T_{11})\, r \tag{30}$$

In order to facilitate the follow-up analysis and experiment, the angle of joint 2 is taken as the system input, and the static friction model in Eq. (14) is replaced by the dynamic friction model:

$$\begin{array}{ll} T_{11} = T_{12} - f_{11,\text{LuGre}} & T_{21} = T_{21} - f_{21,\text{LuGre}} \\ T_{12} = T_p - kr\,(u - \theta_1) & T_{22} = T_p + kr\,(u - \theta_1) \\ T_{13} = T_{12} - f_{12,\text{LuGre}} & T_{23} = T_{12} - f_{22,\text{LuGre}} \end{array} \tag{31}$$

where u is the angle input of joint 2. $f_{(\cdot),\text{LuGre}}$ is the improved LuGre dynamic friction model obtained in the previous section. Combine Eq. (30) and Eq. (31):

$$\tau_c = (2kr\,(u - \theta_1) + f_{11,\text{LuGre}} - f_{21,\text{LuGre}})r \tag{32}$$

The dynamic equation of link 1 is as follows:

$$J\ddot{\theta}_1 + \tau_{f,\text{joint1}} = \tau_c \tag{33}$$

where J is inertia of the link 1. $\tau_{f,\text{joint1}}$ is joint 1 friction, and satisfies the Eq. (27). Define the state variable as follows:

$$\mathbf{x} = \begin{bmatrix} \theta_1 & \dot{\theta}_1 & \mathbf{Z}^T \end{bmatrix}^T \tag{34}$$

where $\mathbf{Z} = \begin{bmatrix} z_{11} & z_{12} & z_{21} & z_{22} & z_{\text{joint}} \end{bmatrix}^T$. The equation of state is obtained:

$$\dot{\mathbf{x}} = \begin{bmatrix} \dot{\theta}_1 \\ \ddot{\theta}_1 \\ \dot{\mathbf{Z}} \end{bmatrix} = \begin{bmatrix} \dot{\theta}_1 \\ \frac{\tau_c - \tau_{f,\text{joint1}}}{J} \\ \mathbf{v} - \sigma_0|\mathbf{v}| \oslash g(\mathbf{v}) \circ \mathbf{Z} \end{bmatrix} \tag{35}$$

where $\mathbf{v} = \begin{bmatrix} r\dot{\theta}_1 & r\dot{\theta}_2 & -r\dot{\theta}_1 & -r\dot{\theta}_2 & \dot{\theta}_1 \end{bmatrix}^T$, $\oslash$ and $\circ$ are Hadamard division and product.

The Runge-Kutta method is used to solve the above first-order differential equation. The system parameters are shown in Table II. The setting of the LuGre parameters of the cable pulley is shown in Table III. The joint friction LuGre parameters define with $\sigma_0 = 1000$, $\sigma_1 = 10$, $v_s = 0.01rad/s$, the others are zero. System input $u = \theta_2(t) = 10sin(0.5\pi t)$.

TABLE II

CCSRM PARAMETERS

Parameter names	Values
Cable elastic coefficient k	$1e6N/m$
Cable initial pretension T_p	$50N$
Pulley radius r	$0.012m$
Initial wrap angle θ_{w0}	$1.69rad$
Link inertia J	$0.01kgm^2$

TABLE III

CABLE-PULLEY LUGRE PARAMETERS

σ_0	σ_1	σ_2	μ_c	μ_s	v_s
1e6	1000	500	0.15	0.18	$5e-5m/s$

Fig. 8(a) shows the simulation results of joint rotation angle and synchronous rotation error. During the start-up phase, the synchronous rotation error gradually increases. This is because the transmission of cable tension to the distal end needs to overcome the friction force first, so that the tension distribution of the cable changes greatly, and the deformation of the cable causes the synchronization rotation error. The error is related to the initial tension distribution of the cable. In the reverse rotation phase, the change of synchronous rotation error approximately equals to the backlash calculated in Eq. (25). Fig. 8(b) shows the

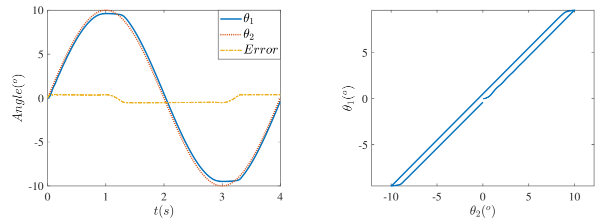

(a) (b)

Fig. 8. Simulation. (a) Joint angle and error. (b) Phase diagram of rotation angle of adjacent joints.

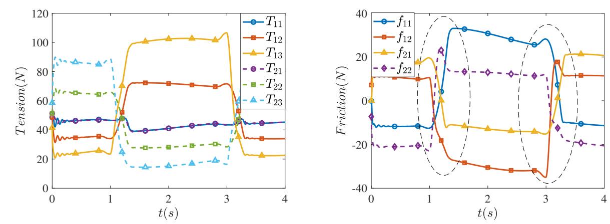

(a) (b)

Fig. 9. Force. (a) Tension distribution of CCP. (b) Cable-pulley friction.

joint rotation angle phase diagram, and the CCSRM shows great hysteresis characteristics.

The tension distribution of CCP is shown in Fig. 9(a). The cable tightens and relaxes alternately during the movement. Fig. 9(b) is the cable-pulley friction, the part inside the dotted line shows the Stribeck phenomenon, which can't be described by static friction model.

V. EXPERIMENT

A. Experiment Setup

As shown in Fig. 10, three tension sensors are installed on each cable. High-precision photoelectric encoder with 17-bit is installed on each joint. Joint 2 is driven by the Maxon motor. The anchor of the cable is equipped with adjustable screws to adjust the pretension force of the cable. A STM32 microcontrollers is used as the controller, which sends instructions to the motor driver through CAN bus, reads the encoder signals through SPI protocol and collects the tension sensor data through ADC.

B. Identification of Cable Elastic Coefficient

The theoretical calculation formula for the elastic coefficient of the cable is $k = EA/l_0$. However, the cable is composed of multiple steel wires with gaps between the wires. And the cable's cross-section area is difficult to calculate accurately. In addition, the cable needs to be pre-stretched before using. Different pre-stretched methods and the gaps in the system will affect the cable's elastic coefficient. Therefore, in general, the elastic coefficient of cable is usually in a range.

In order to obtain accurate cable's elastic coefficient, the synchronous rotation test platform can be used to measure.

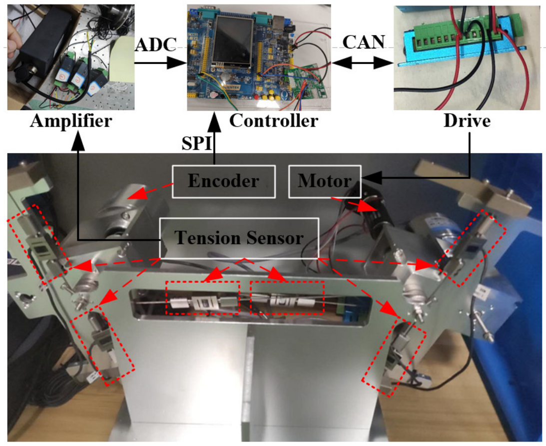

Fig. 10. Experiment prototype.

According to Eq. (14), the cable tension of section L_2 is proportional to the synchronous rotation error of the joint. The proportional coefficient is the elastic coefficient:

$$k = \frac{T_{22} - T_p}{r\Delta\theta} \tag{36}$$

However, the synchronous rotation error of the joint is zero at some moment, the elastic coefficient of cable cannot be obtained directly by the Eq. (36). The MATLAB optimization tool fmincon function is used to identify the elastic coefficient, the objective function is defined as follows:

$$\min \frac{1}{N}\sum_{i=1}^{N}(T_{2,exper}(i) - T_{2,sim}(i))^2 \tag{37}$$

where $T_{2,sim}(i) = t_p + kr\Delta\theta(i)$, $T_{2,exp}$ is the experiment tension data of section L_2 of cable2, N is total number of samples from experimental results.

Since the identification of cable elastic coefficient needs to get the joint synchronous rotation error first, in this experiment, high-precision encoders are installed on both joints to calculate $\Delta\theta(i)$. Manually rotate the joints to collect the corresponding experimental data.

Fig. 11(a) is the experimental data of joint angle and joint synchronous rotation error. When the joint rotates in reverse direction, the joint synchronous rotation error is large and the maximum joint synchronous rotation error is 1.56^o. Fig. 11(b) shows the phase diagram of the adjacent joint angles. It is shown that obvious hysteresis characteristics of the joint motion transmission exists.

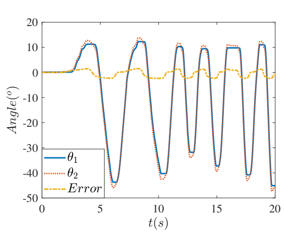

(a)

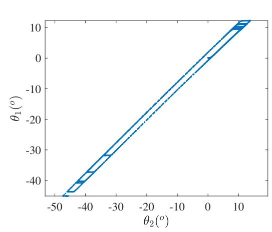

(b)

Fig. 11. Experiment. (a) Joint angle and error. (b) Phase diagram of rotation angle of adjacent joints.

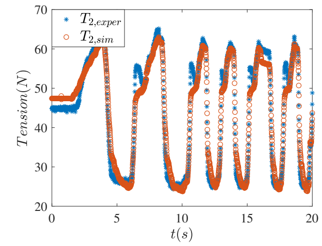

Fig. 12. Tension comparison of cable 2.

The final identification result is $k = 5.023e4N/m$. Fig. 12 shows the comparison between the experimental and the simulation of the cable tension using identification result.

C. Identification of Coulomb Friction Coefficient

From the Eq. (13), the Coulomb friction coefficient is obtained as follows:

$$u_c = \left| \ln\left(\frac{T_{\text{out}}}{T_{\text{in}}}\right)/\theta_{\text{wrap}} \right| \tag{38}$$

Joint 2 is driven by motor, joint 1 is equipped with a high-precision encoder and driven by CCP. Fig. 13(a) shows the rotation angle of joint 1. It can be seen that when joint 2 rotates in the reverse direction, joint 1 will not rotate in the reverse direction immediately. Joint 1 remains stationary for a period of time, that is, a large gap appears during the turning process. Fig. 13(b) shows the change of cable tension distribution.

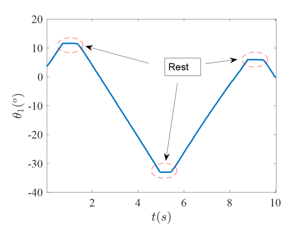

(a)

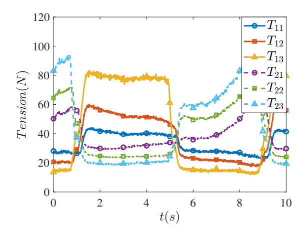

(b)

Fig. 13. Experiment data. (a) The angle of joint 1. (b) Tension distribution.

The result of identification is shown in Fig. 14(a), $u_{c,21}^{+} = 0.178$, $u_{c,21}^{-} = 0.155$. The area with sharp spines corresponds to the reverse rotation process of the joint, so it can be neglected. The cable is composed of multiple steel wires, the contact surface of the cable is different when the cable moves forward and backward, so the friction coefficient is slightly different. In addition, if the friction between cable and pulley is too large, debris will be generated at the contact part after several tests. In order to reduce the friction loss, lubricating oil is added to the contact parts. So the result is smaller than the usually friction coefficient of cable and aluminum, while it does not affect the identification method.

Combined with the dynamic friction coefficient obtained from the identification, the simulation and experiment results are shown in Fig. 14(b), It can be seen that the LuGre friction model can simulate the actual friction well. One possible reason for the difference is that only the deformation of the middle part of the cable is considered in the modeling process.

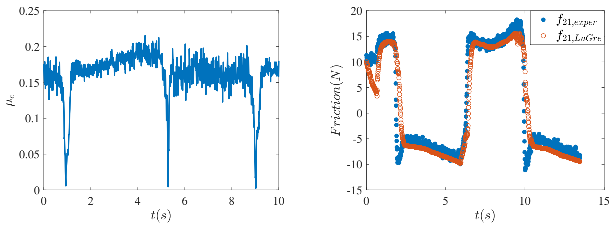

(a) (b)

Fig. 14. Identification. (a) Coulomb friction coefficient identification. (b) Experimental friction and simulated LuGre friction comparison.

VI. CONCLUSION

The CCSRM is an ingenious design that can realize the miniaturization of the synchronizing unit, and realizes approximately synchronous rotation of two joints through two anti-cables. However, the introduction of CCP also greatly increases the complexity of the system. Rotation errors caused by friction between cables and pulleys and elastic deformation of cables will seriously affect the positioning accuracy of robots. The difficulty in modeling CCSRM is the handling of cables. First, we review the design principle of CCSRM, and established the statics model of CCSRM according to the characteristics of cables' arrangement and friction. Then, we improve the LuGre friction model to solve the problem of discontinuous friction in reverse rotation, and establish the dynamic model of CCSRM. The dynamic simulation analysis further proves that the synchronous mechanism has strong hysteresis characteristics. Finally, a synchronous rotating experimental prototype is built, the stiffness coefficient of cable and dynamic friction coefficient in the experimental system are identified. The correctness of the proposed modeling method is verified. We focus on the modeling of CCSRM in this article, in the future, we will continue to study the dynamic modeling and control method of the whole robot system composed of CCSRM.

REFERENCES

[1] M. C. Yip, and D. B. Camarillo, "Model-less hybrid position/force control: a minimalist approach for continuum manipulators in unknown, constrained environments," *IEEE Robot. Autom. Lett*., vol. 1, no. 2, pp. 844-851, 2016.

[2] W. Xu, T. Liu, and Y. Li, "Kinematics, dynamics, and control of a cable-driven hyper-redundant manipulator," *IEEE/ASME Trans. Mechatronics*., vol. 23, no. 4, pp. 1693-1704, 2018.

[3] R. J. Webster III, and B. A. Jones, "Design and kinematic modeling of constant curvature continuum robots: A review," *Int. J. Robot. Res*., vol. 29, no. 13, pp. 1661-1683, 2010.

[4] M. T. Chikhaoui, S. Lilge, S. Kleinschmidt, and J. Burgner-Kahrs, "Comparison of modeling approaches for a tendon actuated continuum robot with three extensible segments," *IEEE Robot. Autom. Lett*., vol. 4, no. 2, pp. 989-996, 2019.

[5] R. Buckingham, and A. Graham, "Nuclear snake-arm robots," *Ind.Robot*., vol. 39, no. 1, pp. 6-11, 2012.

[6] D. Nahar, P. M. Yanik and I. D. Walker, "Robot tendrils: Long, thin continuum robots for inspection in space operations," *2017 IEEE Aerospace Conference*, Big Sky, MT, 2017, pp. 1-8.

[7] R. Buckingham, V. Chitrakaran, R. Conkie, G. Ferguson, A. Graham, A. Lazell, M. Lichon, N. Parry, F. Pollard, and A. Kayani, Snake-arm robots: a new approach to aircraft assembly, 0148-7191, SAE Technical Paper, 2007.

[8] J. Burgner-Kahrs, D. C. Rucker, and H. Choset, "Continuum robots for medical applications: A survey," *IEEE Trans. Robot*., vol. 31, no. 6, pp. 1261-1280, 2015.

[9] S. Huang, D. Meng, Y. She, X. Wang, B. Liang, and B. Yuan, "Statics of continuum space manipulators with nonconstant curvature via pseudorigid-body 3r model," *IEEE Access*, vol. 6, pp. 70854-70865, 2018.

[10] H. Yuan, L. Zhou, and W. Xu, "A comprehensive static model of cable-driven multi-section continuum robots considering friction effect," *Mech. Mach. Theory*., vol. 135, pp. 130-149, 2019.

[11] S. Huang, D. Meng, X. Wang, B. Liang, and W. Lu, "A 3D Static Modeling Method and Experimental Verification of Continuum Robots Based on Pseudo-Rigid Body Theory." in *Proc. IEEE/RSJ Int. Conf. Intell. Robots Syst*., Macau, China, 2019, pp. 4672-4677.

[12] J. Till, V. Aloi, and C. Rucker, "Real-time dynamics of soft and continuum robots based on Cosserat rod models," *Int. J. Robot. Res*., vol. 38, no. 6, pp. 723-746, 2019.

[13] C. Yang, S. Geng, I. Walker, D. T. Branson, J. Liu, J. S. Dai, and R. Kang, "Geometric Constraint Based Modeling and Analysis of a Novel Continuum Robot with SMA Initiated Variable Stiffness," *Int. J. Robot. Res*, 2020.

[14] T. Liu, Z. Mu, W. Xu, T. Yang, K. You, H. Fu, and Y. Li, "Improved Mechanical Design and Simplified Motion Planning of Hybrid Active and Passive Cable-Driven Segmented Manipulator with Coupled Motion," in *Proc. IEEE/RSJ Int. Conf. Intell. Robots Syst*., Macau, China, 2019, pp. 5978-5983.

[15] S. Ma, B. Liang, and T. Wang, "Dynamic analysis of a hyper-redundant space manipulator with a complex cable network," *Aerosp. Sci. Technol*., vol. 100, pp. 105768, 2020.

[16] O. Wallrapp, and S. Wiedemann, "Simulation of deployment of a flexible solar array," *Multibody. Syst. Dyn*., vol. 7, no. 1, pp. 101-125, 2002.

[17] Y. Li, C. Wang, and W. Huang, "Dynamics analysis of planar rigid-flexible coupling deployable solar array system with multiple revolute clearance joints," *Mech. Syst. Signal*. Pr., vol. 117, pp. 188-209, 2019.

[18] Y , Z. Wang, C. Wang, and W. Huang, "Effects of torque spring, CCL and latch mechanism on dynamic response of planar solar arrays with multiple clearance joints," *Acta. Astronaut*., vol. 132, pp. 243-255, 2017.

[19] H.-Q. Li, L.-C. Duan, X.-F. Liu, and G.-P. Cai, "Deployment and control of flexible solar array system considering joint friction," *Multibody. Syst. Dyn*., vol. 39, no. 3, pp. 249-265, 2017.

[20] V. Agrawal, W. J. Peine, and B. Yao, "Modeling of transmission characteristics across a cable-conduit system," *IEEE Trans. Robot*., vol. 26, no. 5, pp. 914-924, 2010.

[21] T. Do, T. Tjahjowidodo, M. W. S. Lau, and S. J. Phee, "A new approach of friction model for tendon-sheath actuated surgical systems: Nonlinear modelling and parameter identification," *Mech. Mach. Theory*., vol. 85, pp. 14-24, 2015.

[22] T.N.Do, T.Tjahjowidodo, M.W.S.Lau, S.J.Pheea, "An investigation of friction-based tendon sheath model appropriate for control purposes," *Mech. Syst. Signal*. Pr., vol. 42, no. 1-2, pp. 97-114, 2014.

[23] T.N.Do, T.Tjahjowidodo, M.W.S.Lau, T.Yamamoto, S.J.Pheea, "Hysteresis modeling and position control of tendon-sheath mechanism in flexible endoscopic systems," *Mechatronics*, vol. 24, no. 1, pp. 12-22, 2014.

[24] V. Agrawal, W. Peine, and B. Yao, "Dual loop control of cable-conduit actuated devices," in *American Control Conference (ACC)*, 2012, pp. 2621–2626.

[25] W. S. Rone and P. Ben-Tzvi, "Continuum robot dynamics utilizing the principle of virtual power," *IEEE Trans. Robot*., vol. 30, no. 1, pp. 275–287, Feb. 2014.

[26] G. Palli and C. Melchiorri, "Model and control of tendon-sheath transmission system," in *Proc. Int. Conf. Robot. Autom*., Orlando, FL, 2006, pp. 988–993.

[27] H. Olsson, K. J. Åström, C. C. de Wit, M. Gafvert, and P. Lischinsky, "Friction models and friction compensation," *Eur. J. Control*, vol. 4, no. 3, pp. 176–195, 1998.